

Double nucleus in M83

Damián Mast¹, Rubén J. Díaz^{1,2}, M.Paz Agüero¹

damian@mail.oac.uncor.edu

ABSTRACT

M 83 is one of the nearest galaxies with an enhanced nuclear star formation and it presents one of the best opportunities to study the kinematics and physical properties of a circumnuclear starburst. Our three-dimensional spectroscopy data in R band confirm the presence of a secondary nucleus or mass concentration (previously suggested by Thatte and coworkers). We determine the position of this hidden nucleus, which would be more massive than the visible one, and was not detected in the optical HST images due, probably, to the strong dust extinction. Using a Keplerian approximation, we estimated for the optical nucleus a mass of $(5.0 \pm 0.8) \times 10^6 M_{\odot} / \sin i$ ($r < 1''.5$), and for the hidden nucleus, located $4'' \pm 1''$ at the NW (PA $271^\circ \pm 15^\circ$) of the optical nucleus, a mass of $(1.00 \pm 0.08) \times 10^7 M_{\odot} / \sin i$ ($r < 1''.5$). The emission line ratio map also unveils the presence of a second circumnuclear ring structure, previously discovered by IR imaging (Elmegreen and coworkers). The data allow us to resolve the behavior of the interstellar medium inside the circumnuclear ring and around the binary mass concentration.

Subject headings: galaxies: individual (M83) – galaxies: kinematics and dynamics – galaxies: nuclei – galaxies: starburst – galaxies: structure – techniques: spectroscopic

1. INTRODUCTION

M 83 is a very special case of nearby grand design barred spiral galaxy (Table 1), it harbors a nuclear X-ray source (Soria et al. 2002), coexisting with a massive starburst

¹Observatorio Astronómico de Córdoba y CONICET, Universidad Nacional de Córdoba, Laprida 854, 5000 Córdoba, Argentina.

²Gemini Observatory, Southern Operations Center, c/o AURA, La Serena, Chile.

in a double circumnuclear ring (Elmegreen et al. 1998) and a secondary mass concentration recently suggested by Thatte et al. (2000) and confirmed by 3D spectroscopic data (Mast et al. 2002). Gallais et al. (1991) obtained infrared (IR) images of the central 20'' in the J , H and K bands and analyzed the color-color diagrams which indicate that the nucleus and several regions in an arc at 7'' from the nucleus are forming stars at a high rate. HST observations (optical and UV) and IUE spectra reveal that the arc contains more than 20 massive young clusters similar to 30 Dor in the Large Magellanic Cloud (LMC), with ages between 2 and 8 million years and masses in the range $1 \times 10^4 - 1 \times 10^6 M_{\odot}$ (Heap et al. 1993; Heap 1994).

Thatte et al. (2000) made IR spectroscopic observations with two long slit positions of the nuclear region using the ISAAC spectrometer at the VLT. They detected two peaks in the radial velocity dispersion profile, one on the K -band luminosity peak, and the other one displaced about 3'' to the SW, suggesting the presence of a secondary nucleus. The lack of two spatial dimensions in the spectroscopic information did not allow them to fix the precise position of the second mass concentration. Although the morphology of the star formation activity has been studied in detail (Gallais et al. 1991; Harris et al. 2001), there are very few kinematic or dynamical studies based in good spatial samplings. In this work we present a study of the 2D kinematics of the central region of this galaxy, which resolves the behavior of the interstellar medium around the binary mass concentration.

2. OBSERVATIONS

A summary of the observations is presented in Table 2. We made three-dimensional (3D) spectroscopic observations of the central region of M 83 using the Multifunctional Integral Field Spectrograph mounted on the 1.54 m telescope at Bosque Alegre Astrophysical Station (Díaz et al. 1999, 2003). The data were gathered between March 2001 and May 2002. Several circumnuclear fields were observed, we present here the analysis of the selected field that includes both mass concentrations.

The analyzed integral field was obtained with a total exposure time of 2 hours. The spectra, with a resolution of 1.5 \AA in the R band, were obtained with an array of 8×14 lenses (1''.5 field each one) sampling a field of $12'' \times 21''$. The seeing was about 2'' so the field is slightly subsampled. We complemented these data with archival HST images in the filters F187N, F190N ($\text{Pa}\alpha$ and $\text{Pa}\alpha$ continuum), F814W (7940 \AA) and F656N (6563 \AA).

3. DATA REDUCTION AND ANALYSIS

The reduction of the spectra was performed with the software SAO (developed by the Special Astrophysical Observatory, Russia), the software ADHOC (Boulesteix 1993) and PC standard worksheets. The procedure followed is described in detail in the works of Díaz et al. (1997), Vega (2000) and Mast (2000). The spectra include the nebular emission lines $H\alpha$, [NII] 6548 Å, 6583 Å, [SII] 6716 Å and 6731 Å which were fitted using gaussian curves to determine the parameters that describe them. In most of the field, the S/N allowed the detection and fitting of the mentioned emission lines, but in some locations (in the field SW border) the S/N ratio of the spectrum was low and only $H\alpha$ and [NII] 6583 Å emission were detected. We made gaussian fitting up to a level of 20% of the peak value. Therein the profile wing asymmetries that in some locations could appear do not affect strongly the manual interactive fitting performed to the lines. Once the emission line gaussian fitting was completed, we obtained the following data for each lens: $H\alpha$, [NII] 6583 Å, [SII] 6717 Å and [SII] 6731 Å fluxes, wavelength positions and FWHM of each line. With this information the following maps were constructed: Red continuum intensity, $H\alpha$ intensity, [NII] 6583/ $H\alpha$, ([SII] 6717+[SII] 6731)/ $H\alpha$, [SII] 6717/[SII] 6731, and FWHM maps. Because the $H\alpha$ line is the most conspicuous emission of the obtained spectra and the one showing better S/N ratio, we only analyzed the radial velocities corresponding to this line. A map of the radial velocity field was also constructed.

As mentioned before, the field was slightly subsampled. In order to improve the data processing and visualization, all the field values were interpolated, yielding the same field sampled by 24×42 elements ($0.5''/\text{pixel}$). The internal error due to the velocity determination procedure has a relative value lower than 5 km sec^{-1} (r.m.s.). That is the precision limit in the velocity field determination, in case we have data with good S/N ratio (> 10). In our case the best S/N ratio in the $H\alpha$ emission line is $S_{Total}/N = 30$, $S_{Peak}/N = 15$; the worst S/N , in one of the outermost lenses, is $S_{Peak}/N = 2$.

4. RESULTS

4.1. Morphological scenario

Figure 1 shows the central $40'' \times 40''$ around the optical nucleus from which a bright small red arc emerges to the SW, but the most conspicuous feature is a giant star forming arc (Gallais et al. 1991; Elmegreen et al. 1998). In this one, to the NE of the nucleus several star clusters are present and have been studied by Harris et al. (2001). Going counterclockwise through the arc, a highly obscured region is located with a large number of dust patches

and a star forming region emerging from the dust, more than $5''$ westward from the nucleus. The R band continuum map (Figure 2) shows an ellipsoidal light distribution with the external isophotes center, determined from the red continuum HST image (F814W filter), located $2''.5$ to the W-SW of the continuum emission peak (PA 230°), which we assumed, corresponds to the optical nucleus position. This result is consistent with the observations of Thatte et al. (2000), who found that the nucleus is not located at the symmetry center (of the circumnuclear light distribution) in their K band images. The symmetry center of the outer isophotes in R and K bands, which could be considered the bulge center, is almost the same, implying that the optical nucleus would be not located at the stellar bulge center (see the sketch in Figure 3).

4.2. Radial Velocity Field of the Ionized Gas

Figure 4 shows the obtained velocity field, which covers $12'' \times 21''$ of the central region of M 83. A square marks the position of the optical nucleus, which corresponds to the continuum image peak (at R band, N_R in Figure 3 and 4). The isovelocity lines were traced each 10 km sec^{-1} (2σ uncertainty). The isovelocity lines are strongly distorted and could indicate a departure from the axisymmetric potential, with a main line crowding at the position indicated by a circle, where the hidden nucleus should be located. The radial velocity field has a distortion that indicates the presence of two mass concentrations, neither of them located exactly on the global velocity field minor axis (dotted line in Figure 4 and 7).

The radial velocity field is similar to that of the central region of NGC 3227 (Arribas & Mediavilla 1994) which shows an AGN out of the kinematic center of the galaxy. A previous clear case of a kinematic center not located at the bar+bulge center of symmetry was found by Díaz et al. (1999) in the 2D spectroscopic maps and images of NGC 1672, a southern barred galaxy with a strong circumnuclear starburst.

The extreme velocity values of the observed field are $V_{max} = 634 \text{ km sec}^{-1}$ and $V_{min} = 542 \text{ km sec}^{-1}$ ($\Delta V = 92 \text{ km sec}^{-1}$).

There is an isovelocity line stretching (Figure 5) which is coincident, within the uncertainties, with the continuum peak previously identified with the optical nucleus, and therefore is about $2''.5$ to the N-NE of the red continuum symmetry center (C_R in Figure 3 and 4).

The radial velocity gradient determined by the line stretching indicates that the mass concentration of the hidden nucleus would be larger than that of the visible one.

Areas with predominant circular motion can be drawn around each mass concentration (see Figure 6). Each area involves 6 lenses (optical nucleus) and 11 lenses (hidden nucleus).

The mass concentration corresponding to the optical nucleus and, within the uncertainties, coincident with the continuum peak position, is at $2''.3 \pm 0''.5$ to the W-SW from the red continuum symmetry center, while the hidden nucleus, kinematically determined, would be at $2''.4 \pm 0''.5$ NW from the red continuum symmetry center. Therefore, the hidden mass concentration is $3''.9 \pm 0''.5$ at PA $271^\circ \pm 15^\circ$, from the optical nucleus (continuum emission peak). Using the astrometric parameters of the HST WFPC observations, we derive the position of the main nucleus: (J2000) $\alpha = 13^{\text{h}} 37^{\text{m}} 00.919^{\text{s}}$, $\delta = -29^\circ 51' 55''.66$ with a $0''.1$ uncertainty. Assuming that this is the position of the peak continuum emission in our maps, the coordinates of the hidden nucleus would be $\alpha = 13^{\text{h}} 37^{\text{m}} 00.540^{\text{s}} \pm 0.04^{\text{s}}$, $\delta = -29^\circ 51' 53''.62 \pm 0''.5$, considering an uncertainty in the position of $1/3$ of sampling element. The position was determined from cosine fitting to the radial velocities azimuthal profiles. The uncertainty is determined by the amount of rotation center displacement that makes the fit clearly wrong. This displacement is about d/\sqrt{n} where d is the sampling element size in arcseconds and n is the number of sampling elements that show a rotation pattern. The hidden nucleus is at the NW extreme of the star formation arc. Its position can be projected on the long slit direction of Thatte et al. (2000), and this projection is at the same position were the authors note a local maximum in the stars velocity dispersion. The main difference is $2''.5$ along a direction perpendicular to the slit of Thatte et al (2000).

The observed region is too small on galactic scale, also perturbed and, in order to derive the kinematic parameters, we smoothed the observed radial velocity field with a median filter of size $6'' \times 6''$. The result is shown in Figure 7. The PA of the minor axis is 138° , very near to the PA of the low resolution CO velocity field determined by Lundgren et al. (2004) of 136° . The masses can be estimated from the Keplerian approximation

$$M \sim 233 V^2 R / \sin i, \quad (1)$$

where i is the inclination, V the velocity in km sec^{-1} , R de radius in pc and M the mass in M_\odot . Therefore we assumed for the masses estimations, an inclination equal to the global inclination value of 24° (Comte 1981). The estimated masses of the nuclei within a $1''.5$ radius would be around $(1.2 \pm 0.2) \times 10^7 M_\odot$ (optical nucleus) and $(2.4 \pm 0.2) \times 10^7 M_\odot$ (hidden nucleus). There is no intention to report strict Keplerian rotation around the mass concentrations, we just note a predominance of circular motions involving several detection elements (lenses) and we derive upper limits for the masses in a Keplerian approximation.

In order to see if the gas is in ordered rotation around the mass concentrations we studied the line profiles: a strongly asymmetric line profile, with pronounced wings on one

side is more likely due to non gravitational motions. As can be seen in Figure 8, this is not the case for the spectra in the hidden nucleus position.

4.3. FWHM map

Figure 6 shows a FWHM map with the radial velocity field superposed. Two local peaks coincident, within the uncertainties, with the position of the two mass concentrations indicated in Figure 4, can be seen. We note here that the lack of exact coincidence between kinematic centers and FWHM peaks, could be real. This is the case of the eccentric disk of M 31 (See Figure 7 of Bacon et al. 2001) where the lack of symmetry in the gravitational potential generates a difference in the locations of the rotation center and the observed velocity dispersion peaks at a given resolution. It is expected that stellar rotation (not gas) around the mass center is not necessary circular because it is subject to perturbations (like the presence of a nearby second nucleus). In this case, the radial velocity dispersion peak is not coincident with the rotation center, due to the ellipticity in the orbits (Bacon et al. 2001; Tremaine 1995). Therefore, the motion is circular only in an approximate approach which allows the mass estimations.

In the SW part of our FWHM map, profile widths exceed 200 km sec^{-1} . This could be due to shocks in the ionized gas considering that this region coincides with the star forming arc.

4.4. [NII] 6583 / $H\alpha$ map

Figure 9 shows the [NII] 6583 / $H\alpha$ ratio. The position of the optical nucleus is marked with a star. A ring of mean value 0.62 is appreciable around the optical nucleus, coincident with the inner ring reported by Elmegreen et al. (1998) (Figure 10). The ratio is comparatively low in the inner ring region (nuclear region) and in the star forming arc, ranging from values between 0.40 in the star forming arc to 0.46 in the inner ring region. Those values are the expected for normal HII regions (lower than 0.5, Osterbrock 1987). The peak value in the ring is $\sim 0.73 \pm 0.02$. Assuming that those ratios depend mainly on the abundance effects, their distribution would indicate that the relative abundance of nitrogen is higher in the ring than in the nuclear region and the star forming arc. The low $I(\lambda 6584)$ in relation to $H\alpha$ would suggests that the starburst in the nuclear region and in the star forming arc is younger than in the ring. The values at the region of $3''$ around the hidden nucleus are $\sim 0.66 \pm 0.02$.

5. DISCUSSION

It is important to note that the circular motion around both regions has been measured within several detection elements. Furthermore the local kinematics suggests that the secondary nucleus is more massive, but another possibility must be mentioned: a warp in the nuclear region could eventually mimic strong distortions of the kinematic minor axis, but the shape of the observed velocity field with two isoline stretchings would be very difficult to reproduce with a mild local change of geometrical parameters and a single warp model. Other possibilities were considered, like the kinematic distortions arisen in bars and spiral arms, but: i) the shape of the radial velocity field cannot be successfully compared with those resulting from numerical modelling like those by Piner et al. (1995) for a barred potential; ii) we do not detect at K band, nuclear bars or spiral arms in the region of the velocity field distortion. In order to yield much greater insight into the physics of the nuclear region, we use the $H\alpha$ and $Pa\alpha$ HST images, together with case B recombination theory, to construct an extinction map of the line emission from the $H\alpha/Pa\alpha$ ratio (Figure 11). This was made in the same way that Harris et al (2001) used the $H\alpha/H\beta$ ratio. Using a two-component model for the dust extinction and following Calzetti (1997), the standard definition of the color excess is

$$E(B - V)_{H\alpha/H\beta} = \frac{\log(R_{obs}/R_{int})}{0.4[\kappa(\lambda_a) - \kappa(\lambda_b)]}, \quad (2)$$

where R_{int} and R_{obs} are the intrinsic and observed hydrogen line ratios, respectively, and $\kappa(\lambda)$ is the extinction curve, measured at the wavelength of the emission line. Using the average LMC curve and a Seaton Galactic curve (Fitzpatrick 1986), and adopting $R_{int} = 0.1$ (Lilly et al. 1987; Osterbrock 1987), we can derive the attenuation in magnitudes from

$$A_{547} = 1.79[E(B - V) - 0.06] + 3.10 \times 0.06 \approx A_V, \quad (3)$$

(from eq.2 of Harris et al. (2001)) where it was assumed a foreground Milky Way component $E(B - V)_{MW} = 0.06$ (Schlegel et al. 1998). According to our extinction map, the values of A_V range from 0 to nearly 7 magnitudes at the region marked in Figure 11.

It can be seen that the strong extinction is very localized and would not play an important role in the kinematics. The position of the hidden nucleus is, within the uncertainties, coincident with a knot appearing at K band (hot spot labelled “region 8” in Figure 8 of Elmegreen et al. (1998)). This could be the IR source corresponding to the hidden mass concentration.

The $H\alpha$ map, not shown here, does not clearly reveal the existence of the innermost circumnuclear ring reported by Elmegreen et al. (1998). Frequently such rings are constituted by a discrete series of emission regions. In this case, the ring is conspicuous in the

near IR color maps presented by Elmegreen et al. (1998) and in our NII/H α map, probably suggesting different properties (mainly age) in the HII regions, instead of an enhanced star formation outside this innermost ring. The most evident H α structure is a star forming arc that extends from the SE to the NW, which would be part of an outermost circum-nuclear ring (Elmegreen et al. 1998). The study of abundances in HII regions in the disks of spiral galaxies has shown the existence of negative gradients with a higher abundance, with the consequence of a higher NII/H α ratio (e.g. Pagel & Edmunds 1981, Evans 1986, Shield 1990). The observed ratios distribution in M 83 could be another example of this phenomenon. Observations of the global trend and the differences between the arms, inter arms and rings regions of the barred galaxy NGC 1566 (Agüero et al. 2004, Roy & Walsh 1986), were interpreted as possibly arisen in different ages of the star forming regions.

One question arises here: if the velocity field distribution corresponds to a binary mass concentration, can the star formation be triggered by the passage of the hidden nucleus trough the high gas density medium? It has been claimed that if a merging satellite galaxy has no nucleus (e.g., Magellanic Clouds), the gas in the satellite will interact with the gas in the host disk and then be settled in the disk before reaching the nuclear region. On the other hand, if it has a nucleus (e.g., M32), the satellite nucleus will sink toward the nuclear region because of the dynamical friction (Taniguchi & Wada 1996). It is assumed that a nucleus is either an SMBH or a significant concentration of a nuclear star cluster. In this respect, satellite galaxies in Mihos & Hernquist (1994) and Hernquist & Mihos (1995) are also nucleated ones. The formation mechanism of the corresponding nuclear starburst and hot-spot nucleus would involve a supermassive binary of compact objects formed by a merger with a nucleated satellite galaxy triggering intense star formation in the central regions of the main spiral galaxy, in which the nuclear gas disk has been formed already by the dynamical effect of the merger itself. As the secondary compact object approaches the nuclear gas disk, the gas disk response to the gravitational perturbation caused by the nonaxisymmetric potential of the binary mass, forming asymmetrical spiral patterns. When the mass of the intruding object is only one-tenth of the primary's, the gas response is so mild that only pseudo-ring features or tightly wound spiral arms are formed in the circumnuclear region. These features are expected to evolve into several H II region clumps, leading to the formation of not very bright hot-spot nuclei. On the other hand, when the mass of the intruding nucleus is comparable to half the primary one, a very strong one-arm spiral shock appears after the close passage of the secondary in each orbital period. The gas clouds are forced to move rapidly into the central region owing to frequent collisions of gas clouds and the starburst is triggered near the nucleus. If this would be the case, then the age gradient in the star-forming arc (see §1) that ends in the hidden nucleus would provide the clue to the dynamical evolution of this complex system.

6. CONCLUSIONS

In this work we studied the morphology, the ionized gas emission and the kinematics in the innermost regions of M 83. A hidden nucleus is not evident in the HST images, although kinematically the radial velocity field points out the presence of a strong mass concentration that could be the mentioned nucleus. Its condition of non detectable source could be due to its location, considering that the kinematically derived position lies close to a strong absorption region ($A_V \sim 7$ mag, see Figure 11).

[NII] emission is relatively lower compared with $H\alpha$ emission of the hidden nucleus region, at what could be the younger end of the starforming arc, according to previous works. This would be consistent with lower metalicity values at this region, but the lack of more emission line ratios precludes a direct confirmation with the data presented here. Notwithstanding, two independent works confirmed through photometry (Harris et al. 2001) the age gradient of this star forming arc. The emission line ratio map also unveils the presence of a second circumnuclear ring structure, previously known by IR imaging (Elmegreen et al. 1998).

Using the Keplerian approximation, the optical nucleus would have a mass of $(5.0 \pm 0.8) \times 10^6 M_\odot / \sin i$ ($r < 1''.5$), and the secondary nucleus, located $(4'' \pm 1'')$ at the NW (PA $271^\circ \pm 15^\circ$) of the optical nucleus, would have mass of $(1.00 \pm 0.08) \times 10^7 M_\odot / \sin i$ ($r < 1''.5$). The FWHM map presents local maxima in the nuclei positions, supporting the conclusion about the presence of two central mass concentrations derived from the radial velocity map.

The behavior of the interstellar medium inside the circumnuclear ring and around the binary mass concentration has been resolved. The hidden nucleus is located on the younger end of the giant arc of star formation; suggesting that the local departure of an axisymmetric gravitational potential would be the trigger of the nuclear starburst in M 83.

7. Acknowledgements

We thank the generous support of Germán Gimeno, Walter Weidmann and Gustavo Carranza during the observations. We also thank the anonymous referee, whose comments allowed us to improve the paper presentation. This research was partially supported by the CONICET (grant PIP 5697), by the Agencia Córdoba Ciencia, and by the Gemini Observatory, which is operated by the Association of Universities for Research in Astronomy, Inc., on behalf of the international Gemini partnership of Argentina, Australia, Brazil, Canada, Chile, the United Kingdom, and the United States of America. Some of the data presented in this paper were obtained from the Multimission Archive at the Space Telescope Science Institute (MAST). STScI is operated by the Association of Universities for Research in As-

tronomy, Inc., under NASA contract NAS5-26555. Support for MAST for non- HST data is provided by the NASA Office of Space Science via grant NAG5-7584 and by other grants and contracts.

REFERENCES

- Agüero, E. L., Díaz, R. J., Bajaja, E., 2004, *A&A*, 414, 453
- Arribas, S., Mediavilla, E., 1994, *ApJ*, 437, 149
- Boulesteix, J. 1993, ADHOC Reference Manual, (Marseille: Pub. De l’Observatoire de Marseille)
- Bacon, R., Emsellem, E., Combes, F., Copin, V., Monet, G., Martin, P., 2001, *A&A*, 371, 409
- Comte, G., 1981, *A&AS*, 44, 1981
- Calzetti, D., 1997, *AJ*, 113, 162
- de Vaucouleurs, G., de Vaucouleurs, A., Corwin, H. Jr., Buta, R., Paturel, G. and Fouque, P., 1991, *Third Reference Catalogue of Bright Galaxies*, Springer, New York.
- Díaz, R., Dottori, H., Carranza, G., Goldes, G., 1999, *ApJ.*, 512, 623
- Díaz, R., Paolantonio, S., Goldes, G., Carranza, G. 1997, *Multifunctional Integral Field-Spectrograph*, *Astronomy Papers* 1/97, Fa.M.A.F., National University of Cordoba, 110 pp.
- Díaz, R., Dottori H., Vera-Villamizar N., Carranza G., 2003, *ApJ*, 597, 860
- Elmegreen, D., Chromey, F., Warren, A., 1998, *AJ*, 116, 2834
- Evans, I. N., 1986, *ApJ*, 306, 544
- Fitzpatrick, E., 1986, *AJ*, 92, 1068
- Gallais, P., Rouan, P., Lacombe, D., Tiphene, D., Vauglin, L., 1991, *A&A*, 243, 309
- Genzel, R., Weitzel, L., Tacconi-Garman, M., Blietz, M., Cameron, M., Krabbe, A., Lutz, D., Sternberg, A., 1995, *ApJ*, 444, 129
- Harris, J., Calzetti, D., Gallagher, J., Conselice, C., Smith, D., 2001, *AJ*, 122, 3046

- Heap, S., 1994, in *Violent Star Formation: from 30 Dor to QSOs*, Ed. G.Tenorio Tagle (Cambridge University Press), 303
- Heap, S., Holbrook, J., Malumuth, E., Shore, S.& Waller, W. 1993, *BAAS*, 182, 3104
- Hernquist, L., Mihos, C., *ApJ*, 1995, 448, 41
- Lilly, S. J., Hill, G. J., 1987, *ApJ*, 315, 103
- Lundgren, A., Olofsson, H., Wiklind, T., Rydbeck, G., 2004, *A&A*, 422, 865L
- Mast, D., Díaz, R.,Agero, M.P., Weidmann, W., Gimeno, G., 2002, *Espectroscopía de Campo Integral de la Región Central de NGC 5236*, BAAA No. 45
- Mast D., 2002, Master level dissertation, National University of Córdoba. See abstract in Mast et al. 2002
- Mihos, C., Hernquist, L., *ApJ*, 1994, 425L, 13
- Oddone M. A., Goldes G., Carranza G., Díaz R., Plana, Boulesteix, 1999, *BAAA* 43, 70
- Osterbrock, D. E. 1987, *Astrophysics of Gaseous Nebulae and Active Galactic Nuclei*, University Science Books
- Pagel, B. E. J., Edmunds, M. G., 1981, *ARA&A*, 19, 77
- Piner, G., Stone, J., Teuben, P., 1995, *ApJ*, 449, 508
- Roy, J., Walsh, J., 1986, *MNRAS*, 223, 39
- Schlegel, D. J., Finkbeiner, D. P., & Davis, M., 1998, *ApJ*, 500, 525
- Shields, G. A., *ARA&A*, 28, 525
- Soria, R., Wu, K., 2003, *A&A*, 410, 53
- Taniguchi, Y., Wada, K., 1996, *ApJ*, 469, 581
- Thatte, N., Tecza, M., Genzel, R., 2000, *A&A*, 364, L47
- Tremaine, S., 1995, *AJ*, 110, 628
- Vega, L., Díaz, R. J., Lípari, S., Storchi-Bergmann, T., Dottori, H., 2000, *Cinemática y Espectrofotometría de NGC 5248*, No. 44 BAAA, p.68

Vega L., 2000, Master level dissertation, National University of Córdoba. See abstract in Vega et al. 2000

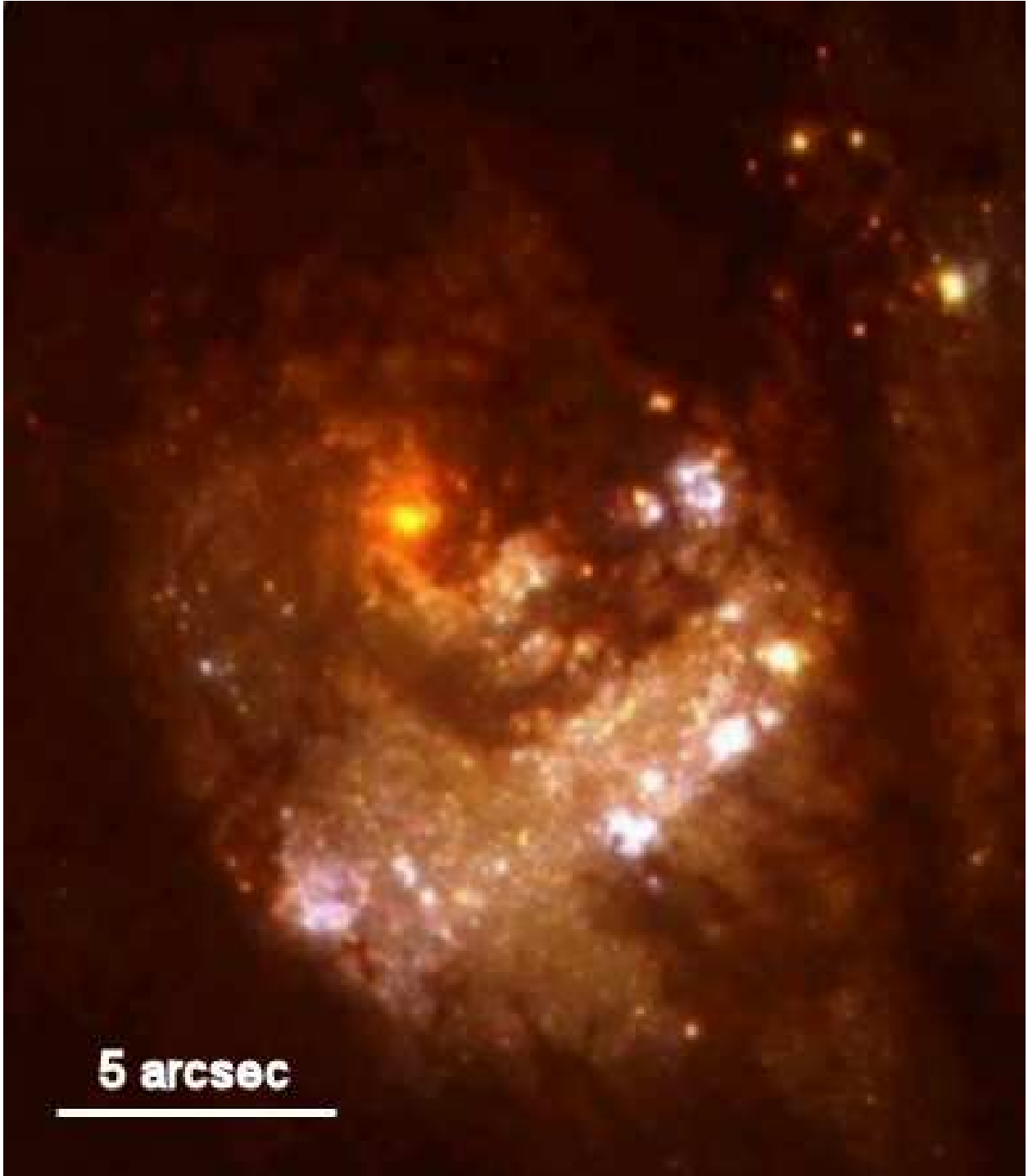


Fig. 1.— HST false color image combined from F439W (contributing to the white-bluest features in the representation), F555W (yellow) and F702W (contributing to the reddest features of the depiction). Point spread functions were matched to a common resolution of $0''.09$. North is at the top and east is at the left.

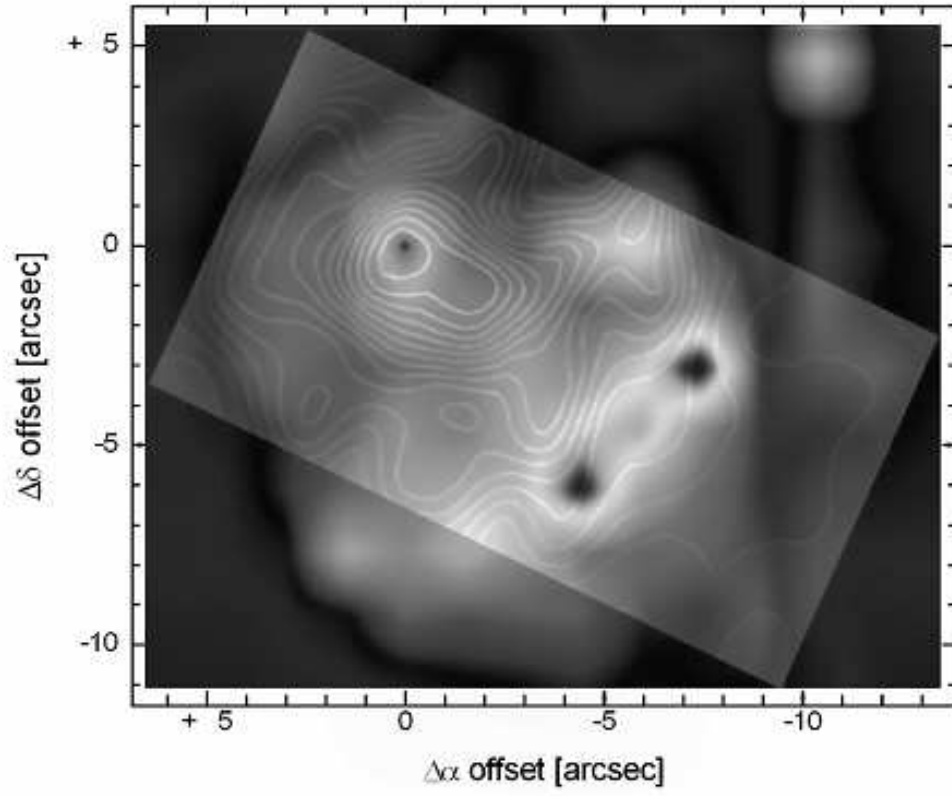


Fig. 2.— Map of red continuum relative intensity (isophotes) computed in the range 6454 – 6524 Å, superposed to F814W HST image smoothed to 1'' seeing.

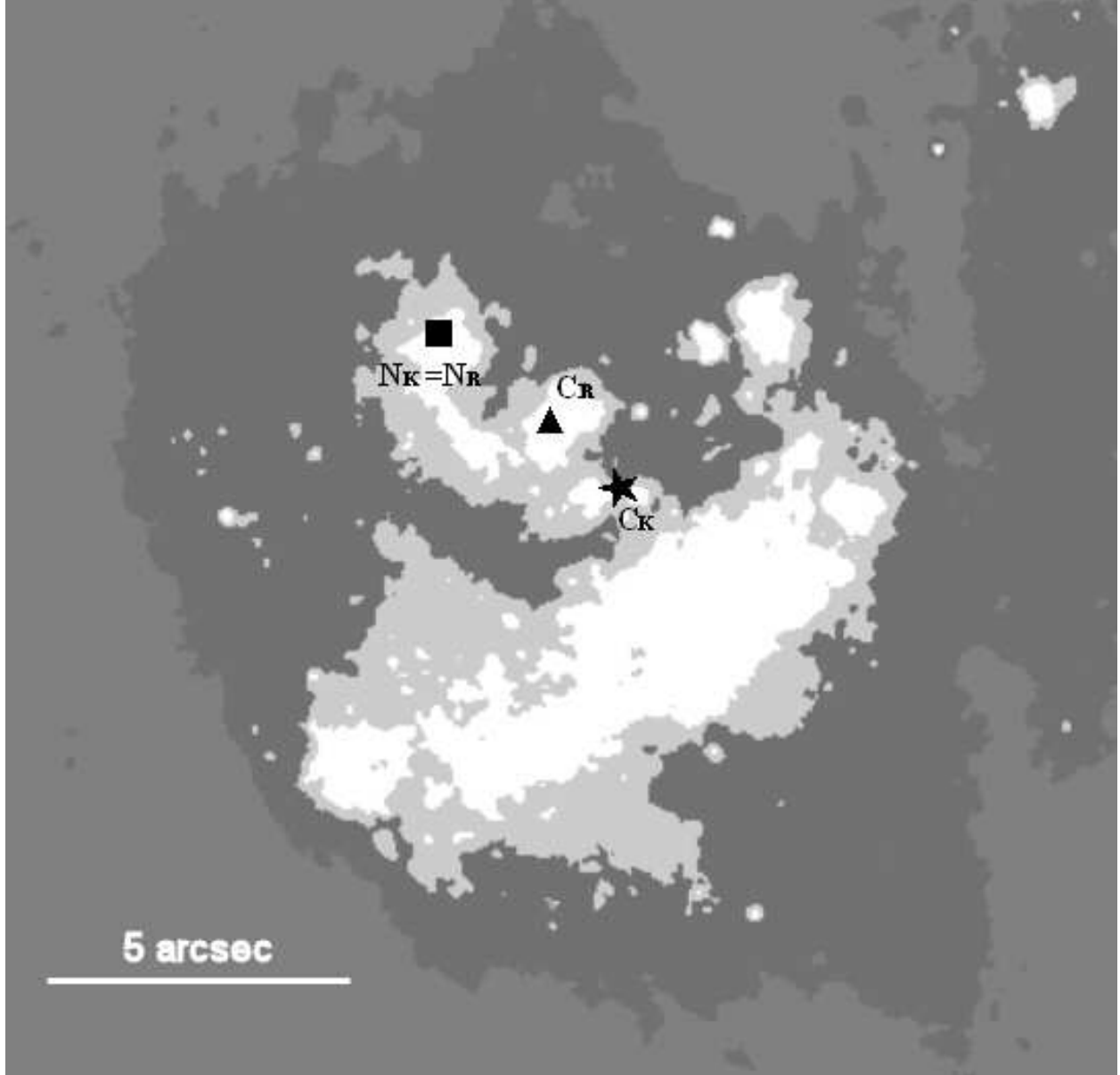


Fig. 3.— Sketch of NGC 5236 central region. North is at the top and east is at the left. A square marks the position of the optical nucleus, which corresponds to the continuum image peak (at R band, N_R). A triangle marks the position of the red continuum symmetry center (C_R). A star marks the position of the symmetry center of the outer isophotes (bulge) in the K band image (C_K).

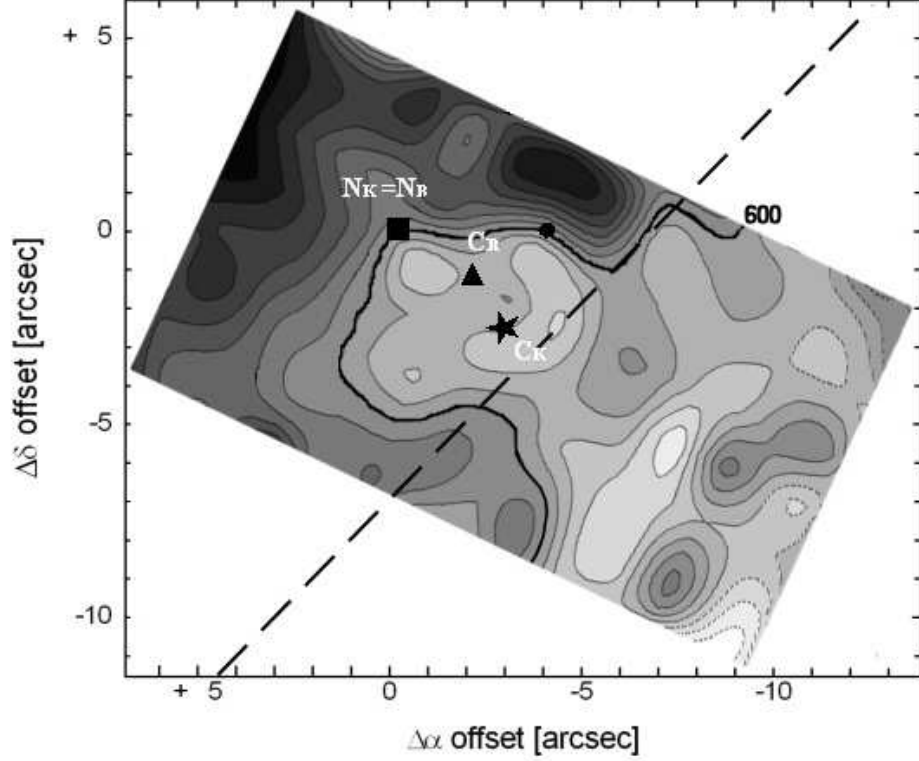


Fig. 4.— $H\alpha$ radial velocity field. A square indicates the position of the optical nucleus and a circle marks the position of the hidden mass concentration. The isovelocities are depicted each 10 km sec^{-1} (2σ uncertainty). The highest and lowest values are 634 km sec^{-1} and 542 km sec^{-1} , respectively. Dark is blueshift and light is redshift. A thicker contour corresponds to the systemic velocity. The dotted line marks the global minor axis at PA 136° . The isovelocity contours with less robust S/N values have been marked with dotted lines.

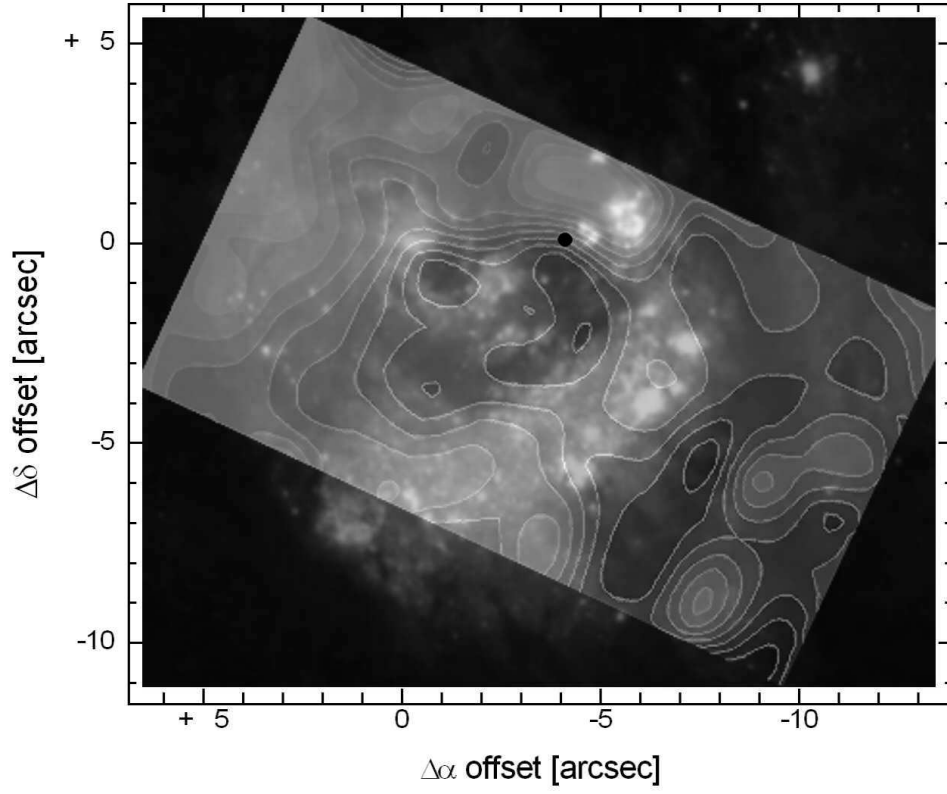


Fig. 5.— H α radial velocity field + HST grey scale image. Note the line stretching coincident with the continuum peak. A circle marks the position of the hidden mass concentration. Contour levels are the same as in Fig. 4.

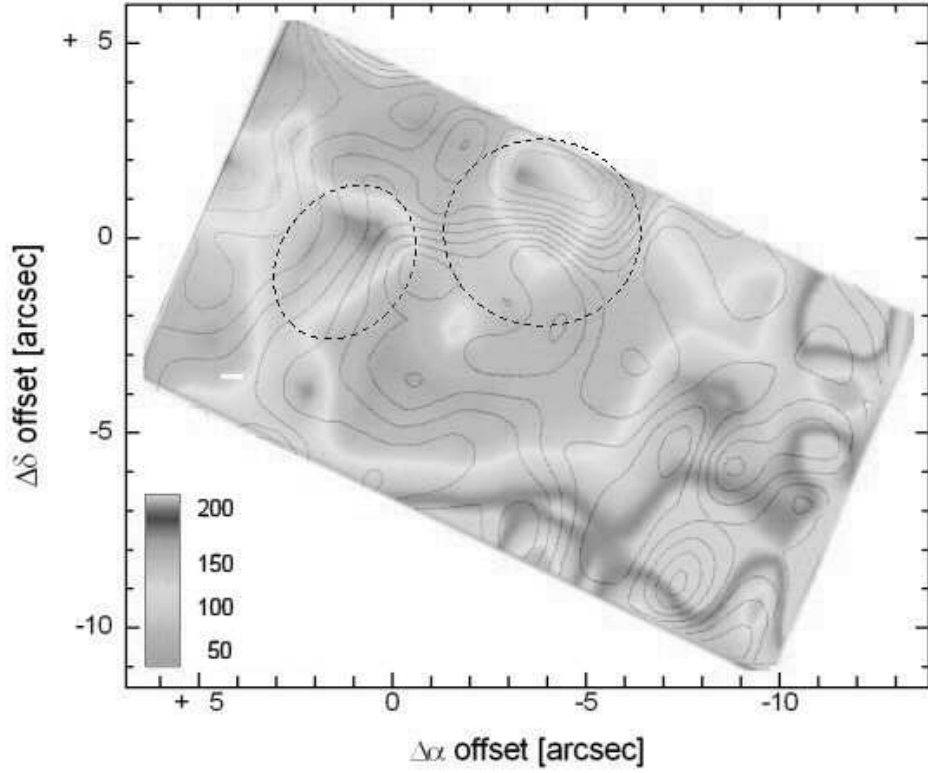


Fig. 6.— Distribution of radial velocity FWHM, the highest values are depicted dark. The isolines correspond to the $H\alpha$ velocity field. The darkest zones correspond to $\text{FWHM} \sim 200 \text{ km sec}^{-1}$. Areas with predominant circular motion are drawn with dotted lines. In the grey zones with values below 100 km sec^{-1} (in white) the line widths are not distinct from the instrumental profile. The inset scale is in km sec^{-1} .

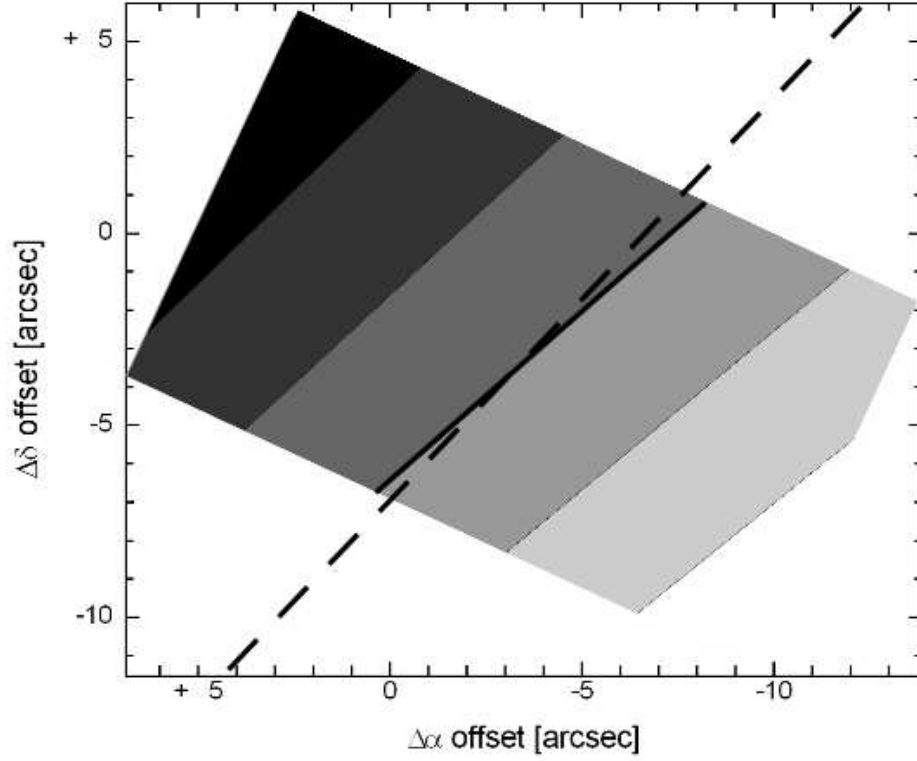


Fig. 7.— Smoothed ($6'' \times 6''$) radial velocity field. The isovelocities are depicted each 20 km sec^{-1} . The minor axis PA of the resultant smoothed field is 132° . A thick contour marks the systemic velocity. Also drawn with a dotted line is the global CO velocity field minor axis PA of 136° (Lundgren et al. 2004).

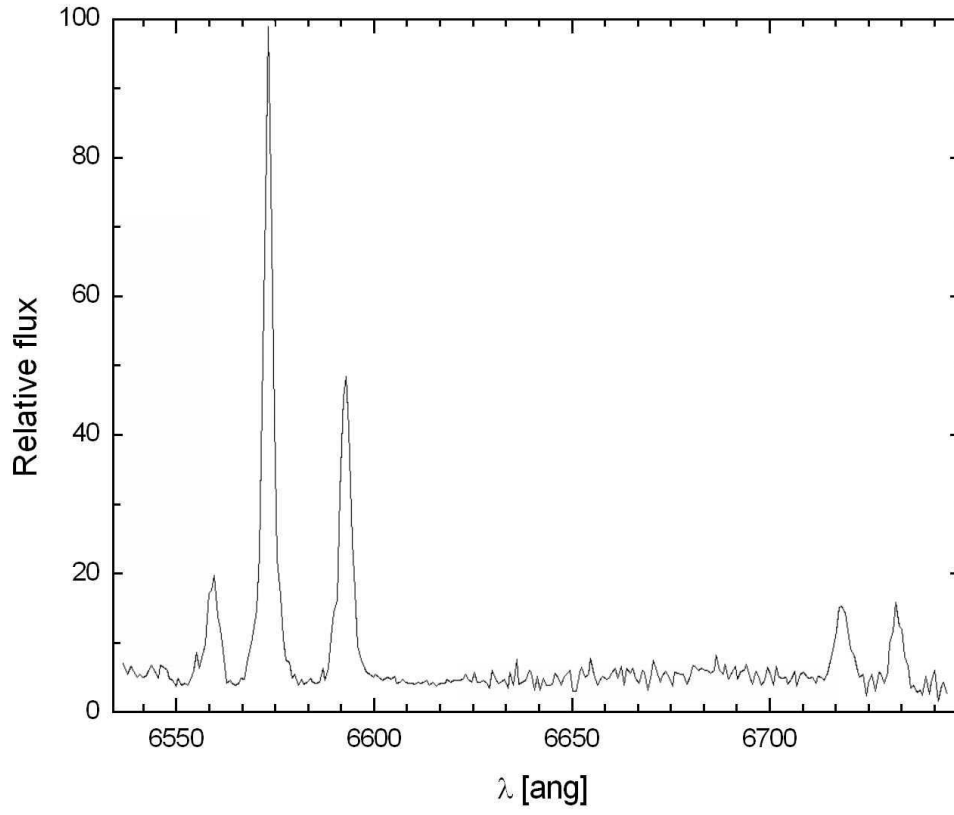


Fig. 8.— Spectra of a single sampling element from the hidden mass concentration region. Note that there are not strong asymmetries in the line profiles.

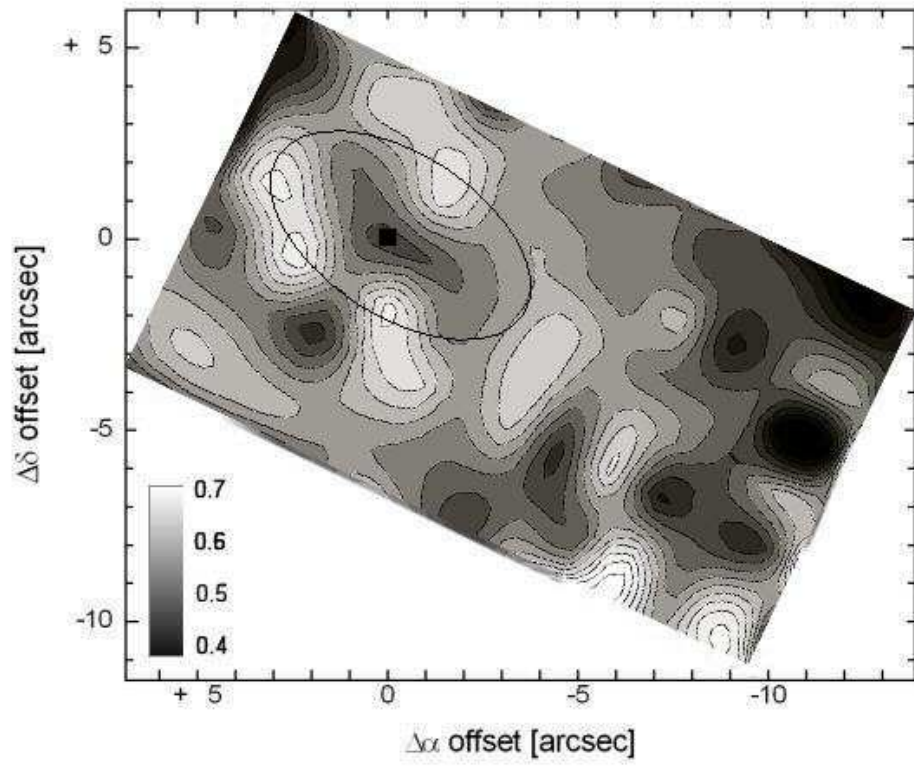


Fig. 9.— NII/H α ratio map. The peaks of NII/H α ratio > 0.6 (lightest in the figure) are surrounded by a dark contour. A square marks the position of the optical nucleus.

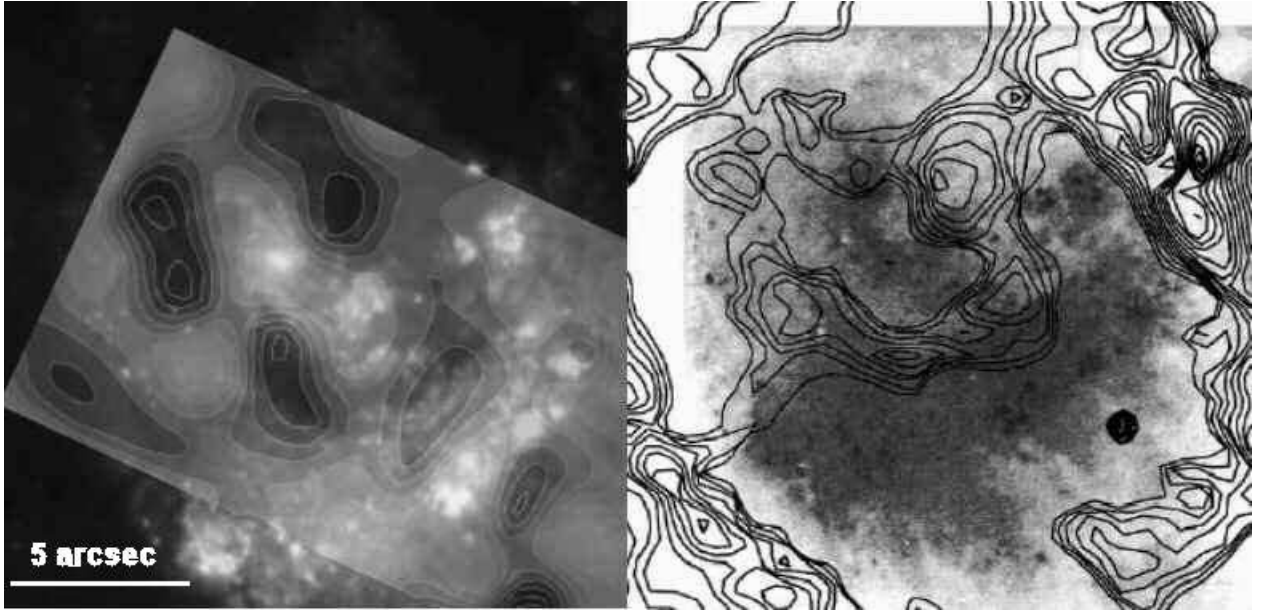


Fig. 10.— *Left.* NII/H α ratio map superposed to the grey scale HST image. *Right.* $(J - K)$ unsharp-masked contours overlaid on an HST V-band image by Heap (1994) (Figure 5 from Elmegreen et al. 1998).

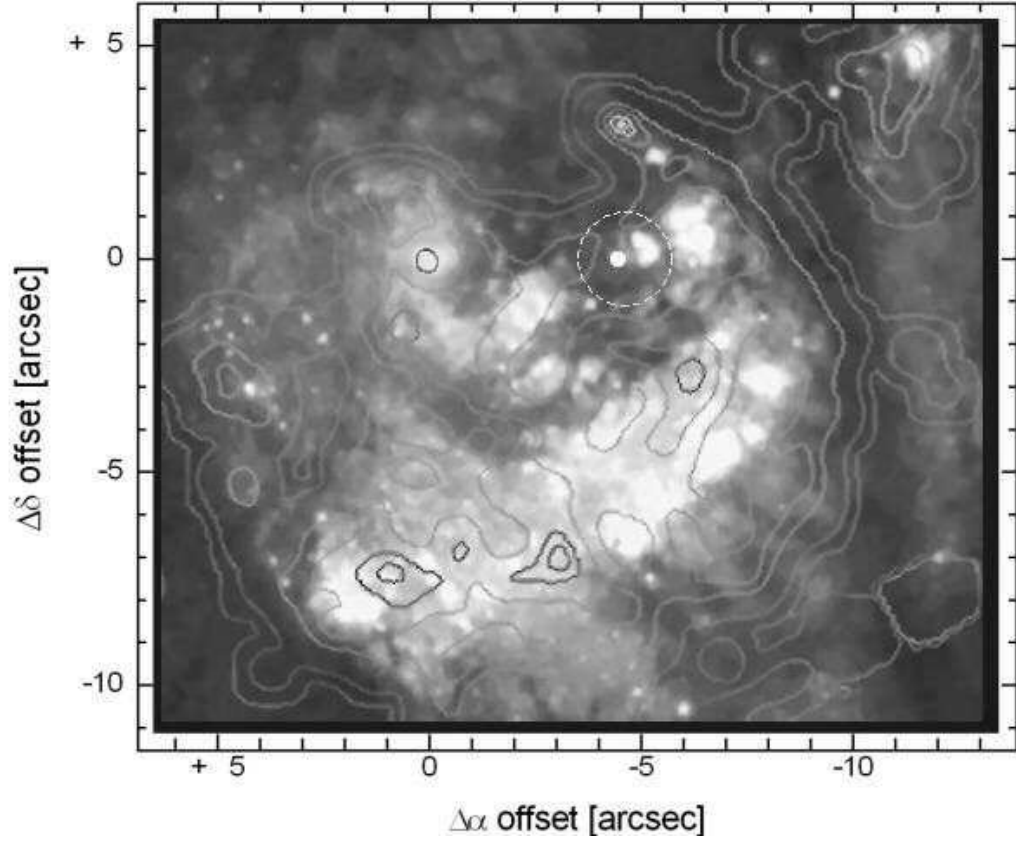


Fig. 11.— Line emission extinction map generated from the $\text{Pa}\alpha/\text{H}\alpha$ HST images ratio (contours) overlaid on a gray scale HST image. Contours values range from 0.15 at the optical nucleus (dark contours), which correspond to $A_V = 0.9$ mag to 2.3 at $(\Delta\alpha; \Delta\delta) = (-5''; 2''.5)$ (light contours), which correspond to $A_V = 6.8$ mag. A white circle marks the position of the hidden mass concentration and a dotted circle marks the uncertainty in its location.

Table 1. M 83 Characteristics

Feature		Reference
V_{\odot}	503 km sec ⁻¹	¹
M	-20.4	¹
Size	12'.9 × 11'.5	^{1, 2}
B_T	8.20 mag	^{2, 3}
D (h = 0.75)	3.7 Mpc	³
Kinematic major axis	PA 46°	⁴
i	24°	⁵
Inner CN ring radius	2.8'', 51 pc	⁶
Outer CN ring radius	8.6'', 152 pc	⁶
Bar length	354'', 6 kpc	⁷

¹Oddone 1999

²Measured at $\mu_B = 25 m_B \text{ arcsec}^{-2}$

³RC3, de Vaucouleurs et al. 1991

⁴undgren et al. 2004

⁵Comte 1981

⁶Elmegreen et al. 1998

⁷DSS image

Table 2. Log of Observations

	Date	Exp.Time [sec]	λ_0 [Å]	$\Delta\lambda$ [Å]	PA [deg]	Pixel scale	Field of view [arcsec]	Comments
HST	May 2000	600	6563	21	209°	0'049	160'' × 160''	H α image
HST	April 2000	160	7940	1531	209°	0'049	160'' × 160''	Red continuum image
HST	May 1999	160	18739	187	212°	0'075	19''2 × 19''2	Pa α image
BAlegre	May 2002	3600	6600	800	96°	1''5, 0.78 Å	12'' × 21''	Integral Field
BAlegre	May 2002	3600	6600	800	96°	1''5, 0.78 Å	12'' × 21''	Integral Field

Note. — BAlegre: Estación Astrofísica de Bosque Alegre.